

---

# Continual Prototype Evolution: Learning Online from Non-Stationary Data Streams

---

**Matthias De Lange**

KU Leuven

[matthias.delange@kuleuven.be](mailto:matthias.delange@kuleuven.be)

**Tinne Tuytelaars**

KU Leuven

[tinne.tuytelaars@kuleuven.be](mailto:tinne.tuytelaars@kuleuven.be)

## Abstract

As learning from non-stationary streams of data has been proven a challenging endeavour, current continual learners often strongly relax the problem, assuming balanced datasets, unlimited processing of data stream subsets, and additional availability of task information, sometimes even during inference. In contrast, our continual learner processes the data streams in an online fashion, without additional task-information, and shows solid robustness to imbalanced data streams resembling a real-world setting. Defying such challenging settings is achieved by aggregating prototypes and nearest-neighbour based classification in a shared latent space, where a Continual Prototype Evolution (CoPE) enables learning and prediction at any point in time. Learning is facilitated by a novel objective function, encouraging cluster density about the class prototype and increased inter-class variance. On top of that, the latent space quality is further elevated by exploiting pseudo-prototypes in each batch. As the embedding network continually changes, prototypes inevitably become obsolete, which we prevent by replay of exemplars from memory. We obtain state-of-the-art performance by a significant margin on five benchmarks, including two highly unbalanced data streams.

## 1 Introduction

The prevalence of data streams in contemporary applications urges systems to learn in a continual fashion. Autonomous vehicles, sensory robot data, and video streaming yield never-ending streams of data, with abrupt changes in the observed environment behind every vehicle turn, robot entering a new room, or camera cut to a subsequent scene. Alas, learning from streaming data is far from trivial due to these changes, as neural networks tend to forget the knowledge they previously acquired. The data stream presented to the network is not identically and independently distributed (iid), emanating a trade-off between neural stability to retain the current state of knowledge and neural plasticity to swiftly adopt the new knowledge [10]. Finding the balance in this stability-plasticity dilemma addresses the catastrophic forgetting induced by the non-iid intrinsics of the data stream, and is considered the main hurdle for continually learning systems.

On top of that, fully exploiting the ceaseless stream of data requires rapid processing, for which *online* continual learning considers only small data batches at a time. This is in strong contrast to a major body of work in task-incremental continual learning [7], which sequentially processes large chunks of data that are accessed simultaneously and for multiple epochs. The data streams are often assumed to be balanced with an equal amount of data for each task, whereas we argue that the frequency of occurrence for categories remains unpredictable in real-world data streams. Furthermore, the artificially delineated task-boundaries introduce a bias by design, and typically hold the unrealistic assumption the task to which a sample belongs to is a given.

These myriad assumptions restrict continually learning systems to limited practical use, as real-world applications require online processing of data, ignorance to the notion of task, and robustness to

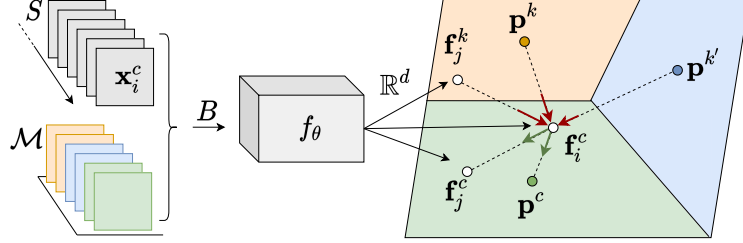


Figure 1: Main setup with embedding  $f_\theta$  mapping input batch  $B$ , composed of samples from the non-iid data stream  $S$  and replay memory  $M$ , to low-dimensional  $\mathbb{R}^d$  latent space. Replay from buffer  $M$  maintains the representativeness of the prototypes, with the PPP-loss encouraging inter-class variance (red arrows) and reducing intra-class variance (green arrows).

imbalanced data streams. To establish such a system, we advocate the use of prototypes in CoPE to continually represent the class distributions in a learned latent space. The prototypes perpetually represent the most salient features of the parent population, shifting the catastrophic forgetting problem from the full parameter space of the network to the low-dimensional latent space. As their parameters are decoupled from the embedding network, interference between classes is drastically reduced. Prediction in CoPE resembles the representativeness heuristics in human cognition [18] by considering similarity to these prototypes for nearest neighbour classification. As a consequence, both learning and prediction can be established at any given point in time, which is key to establish a true continual learner. The embedding network projecting samples to latent space has two additional advantages. First, the latent space enables exploiting positive and negative pairs in the current batch. These pairs constitute pseudo-prototypes to control latent population density and enhance inter-class variance with our Pseudo-Prototypical Proxy (PPP) objective function. Second, in contrast with the typical softmax classifier, the embedding network has a prediction head with fixed capacity, inherently able to incorporate an infinite number of categories without changing the architecture.

Recent works addressing online continual learning have mostly relied on capacity expansion of the model [31, 23] or replay from memory with focus on replacement schemes [22] and sampling strategies [2]. We also incorporate replay of exemplars to prevent the prototypes becoming obsolete, but avoid the need for careful memory replacement and sampling schemes as the exemplar subpopulation is only required to approximate the class mean in latent space. In contrast to the capacity expansion based methods, we evade unbound allocation of resources, as the memory and network capacity are fixed with the replay memory dynamically subdivided over categories occurring in the data stream. Note that new categories require an additional prototype, but these are only  $d$ -dimensional and therefore insignificant in size, and the set of categories is typically limited as well.

Although using prototypes in continual learning has been proposed in iCaRL [32], these are only used for prediction, and are independent of the task based softmax training. Moreover, prediction requires exhaustive recalculation of all prototypes with the full replay memory. Conversely, our approach is the first to concurrently enable prototype-based training and prediction at any point in time, without task knowledge, and in an online fashion. Prototypes evolve continually and are the cornerstone to our novel Pseudo-Prototypical Proxy loss, which additionally exploits current batch instances.

## 2 A prototypical approach

### 2.1 Task-free online continual learning

The main setup is illustrated in Figure 1, where the continual learner is presented an indefinite stream of data  $S$ , processed in small batches and without indication to which specific task incoming samples adhere. Data stream  $S$  is typically highly non-iid, leading to catastrophic forgetting upon distribution shifts. A small online processing buffer stores the most recent  $|B_n|$  samples of the stream, from which the batch  $B_n = \{(\mathbf{x}_1, y_1), \dots, (\mathbf{x}_{|B_n|}, y_{|B_n|})\}$  is fully sampled, with data entries  $(\mathbf{x}_i, y_i)$  constituting the input sample  $\mathbf{x}_i$  and corresponding supervision signal  $y_i$ . The final network layer constitutes a single head, shared among all observed classes  $C$ , with each class represented by a single prototype. Our architecture projects the input data into latent space, in which nearest neighbour classification is performed based on the class-specific prototypes. We assume the number of classes for a true

continual learner to remain unknown a priori. In a softmax classifier this requires extending capacity with additional output nodes as  $C$  grows, whereas our nearest neighbour classifier retains a fixed  $d$ -dimensional latent space regardless of the number of observed classes.

## 2.2 Prototypical replay

The main objective is to learn the embedding network  $f_\theta : \chi \rightarrow \mathbb{R}^d$  parameterized by  $\theta$ , mapping the input space  $\chi$  to a  $d$ -dimensional latent space. The network generalizes shared knowledge in this latent space about all classes in data stream  $S$ . We enforce  $\|f_\theta(\mathbf{x}_i)\| = 1$  with an L2 normalization layer. In the following,  $\mathbf{f}_i^c$  will denote latent space projection  $f_\theta(\mathbf{x}_i^c)$  for an instance  $\mathbf{x}_i$  of class  $c$ .

In order to fence off catastrophic forgetting, each observed class  $c \in C$  is represented by a slowly progressing prototype  $\mathbf{p}^c$ . Then, at prediction  $\mathbf{p}^c$  is used for a nearest neighbour classifier to find the most similar prototype for the given query  $\mathbf{x}_i$ , predicting  $c^* = \arg \max_{c \in C} \mathbf{f}_i^c \mathbf{p}^c$ . Similar to [28, 32], the class-prototype approximates the center of mass in the latent space.

The main crux with shifting data distributions is to prevent the prototypes becoming obsolete. As the samples of class  $c$  shift from the mode to the tail of the underlying class distribution in  $S$ , the embedding changes with the assumed representative  $\mathbf{p}^c$  drifting away from the actual center of mass. To overcome this challenging issue, we add the following key components. First, a replay buffer  $\mathcal{M}$  enables rehearsal of previously observed samples to rectify approximation  $\mathbf{p}^c$  to the true center of mass. Concretely, the sampled batch  $B_n$  from the data stream  $S$  joins a batch  $B_{\mathcal{M}}$  of equal size from the memory, constituting  $B$  as  $B_n \cup B_{\mathcal{M}}$ . Additionally, the prototype is prone to high momentum based updates, aiming to stabilize the impetuous changes in the data stream:

$$\mathbf{p}^c \leftarrow \alpha \mathbf{p}^c + (1 - \alpha) \bar{\mathbf{p}}^c, \text{ s.t. } \bar{\mathbf{p}}^c = \frac{1}{|B^c|} \sum_{\mathbf{x}^c \in B^c} f_\theta(\mathbf{x}^c), \quad (1)$$

with momentum parameter  $\alpha \in [0, 1]$ , the batch subset  $B^c = \{(\mathbf{x}_i, y_i = c) \in B\}$  of class  $c$ , and  $\bar{\mathbf{p}}^c$  the corresponding center of mass in latent space for the current batch.

Following [32], the total buffer size  $M$  is equally divided over the number of observed classes  $|C|$  in a dynamic fashion. This scheme ensures consistent buffer capacity for all classes, making memory population independent of the data stream characteristics. As  $S$  is typically highly unbalanced in real-world scenarios, this memory scheme prevents classes to be eradicated from the buffer, and assumes equal importance to represent each class at all times. Consequently, random retrieval from the buffer resembles sampling an iid replay batch over the memory. Furthermore, each class-specific memory  $\mathcal{M}^c$  can simply capture a random subset of its parent class distribution to approximate its center of mass. This avoids computationally expensive herding techniques as in iCARL [32], which require recalculation of the feature means on each change of the memory size or network parameters.

## 2.3 Pseudo-Prototypical Proxy loss

Optimizing the embedding network  $f_\theta : \chi \rightarrow \mathbb{R}^d$  aims to project an instance  $\mathbf{f}_i^c \in \mathbb{R}^d$  of class  $c$  close to its corresponding prototype  $\mathbf{p}^c$  for the nearest mean classifier. As the prototype acts as a surrogate for the class mean in latent space, the cluster population has a common reference point to reduce intra-class variance. Furthermore,  $\mathbf{f}_i^c$  should remain distant from the other class prototypes, which we can exploit to enforce inter-class variance.

Additionally, due to the embedding architecture we can use the intrinsic information of batch  $B$  in the latent space. The supervision signal  $y_i$  in a sample  $(\mathbf{x}_i, y_i) \in B$  not only indicates which class the sample  $\mathbf{x}_i$  belongs to, but also makes the distinction between positive and negative pairs in  $B$ . Consequently, we can define one-against-all subsets for an instance of class  $c$ , with positives from the same class in  $B^c = \{(\mathbf{x}_i, y_i = c) \in B\}$  and negatives in  $B^k$  with  $k \neq c, \forall k \in C$ . Then, we define the expected posterior probability of sample  $\mathbf{x}_i^c$  to be recognized as an instance of class  $c$  as

$$P(c|\mathbf{x}_i^c) = \mathbb{E}_{\tilde{\mathbf{p}}^c \in S_{pos}^c} [P(c|\mathbf{f}_i^c, \tilde{\mathbf{p}}^c)], \quad S_{pos}^c = \{\mathbf{p}^c\} \cup \{\hat{\mathbf{p}}^c = f_\theta(\mathbf{x}_j^c) \mid \forall \mathbf{x}_j^c \in B^c, i \neq j\} \quad (2)$$

with  $B^c$  introducing the remaining instances of class  $c$  as pseudo-prototypes  $\hat{\mathbf{p}}^c$  to decrease intra-class variance, and  $\mathbf{p}^c$  safeguarding the absence of positive batch pairs by guaranteeing  $1 \leq |S_{pos}^c| \leq |B^c|$ . In Eq. 2, the expectation over pseudo-prototypes and the prototype in  $S_{pos}^c$  is defined over  $P(c|\mathbf{f}_i^c, \tilde{\mathbf{p}}^c)$

with  $\tilde{\mathbf{p}}^c$  a proxy for the latent mean of class  $c$  in

$$P(c|\mathbf{f}, \tilde{\mathbf{p}}^c) = \frac{\exp(\mathbf{f}^T \tilde{\mathbf{p}}^c / \tau)}{\exp(\mathbf{f}^T \tilde{\mathbf{p}}^c / \tau) + \sum_{k \neq c} \exp(\mathbf{f}^T \mathbf{p}^k / \tau)} \quad (3)$$

with temperature  $\tau$  controlling the concentration level of the distribution [15]. In this work, we assume a cosine similarity metric  $\mathbf{f}_i^T \mathbf{f}_j$  with vectors normalized to unit length.

Further, the batch contains  $|B^k|$  negative pairs with  $\mathbf{x}_i^c$ , for which each instance  $\mathbf{x}^k \in B^k$  should both repel  $\mathbf{p}^c$  to avoid being classified as  $c$ , and push off  $\mathbf{f}_i^c$  to increase inter-class variance. Hence, the probability for faulty classification of  $\mathbf{x}_j^k$  as class  $c$  is

$$P_i(c|\mathbf{x}_j^k) = \mathbb{E}_{\tilde{\mathbf{p}}^c \in S_{neg}^c} [P(c|\mathbf{f}_j^k, \tilde{\mathbf{p}}^c)], \quad S_{neg}^c = \{\mathbf{p}^c, \tilde{\mathbf{p}}^c = f_\theta(\mathbf{x}_i^c)\} \quad (4)$$

with  $P(c|\mathbf{f}_j^k, \tilde{\mathbf{p}}^c)$  following Eq. 3, and  $\mathbf{f}_i^c = f_\theta(\mathbf{x}_i^c) \in S_{neg}^c$  acting as pseudo-prototype.

Similar to [37], we formulate a binary classification problem, with the joint probability that instance  $\mathbf{x}_i^c$  is predicted as class  $c$  and instances  $\mathbf{x}_j^k$  not being predicted as class  $c$

$$P_i = P(c|\mathbf{x}_i^c) \prod_{\mathbf{x}_j^k} (1 - P_i(c|\mathbf{x}_j^k)) \quad (5)$$

with the assumption of independence between  $\mathbf{x}_i^c$  and  $\mathbf{x}_j^k$  being recognized as  $c$ . We reformulate this objective as loss function  $J$  by negative log likelihood and summation over all the instances in  $B$ , which approximates the true joint probability with assumed independent pairs in the batch:

$$J = -\frac{1}{|B|} \left[ \sum_i \log P(c|\mathbf{x}_i^c) + \sum_i \sum_{\mathbf{x}_j^k} \log(1 - P_i(c|\mathbf{x}_j^k)) \right]. \quad (6)$$

## 2.4 Optimal prototypes

We update prototypes to approximate the mean of the parent distribution in Eq. 1. This assumption is optimal for Bregman divergences for which the cluster mean is shown to have minimal distance to its population [4]. This Bregman divergence is defined for a differentiable, strictly convex function  $\varphi$  as

$$d_\varphi(\mathbf{f}_i, \mathbf{f}_j) = \varphi(\mathbf{f}_i) - \varphi(\mathbf{f}_j) - (\mathbf{f}_i - \mathbf{f}_j)^T \nabla \varphi(\mathbf{f}_j), \quad (7)$$

for which the squared Euclidean distance with  $\varphi(\mathbf{f}) = \|\mathbf{f}\|^2$  is a canonical example. The squared Euclidean distance is proportional to the cosine distance with vectors normalized to unit length:  $\frac{1}{2} \|\mathbf{f}_i - \mathbf{f}_j\|^2 = 1 - \cos \angle(\mathbf{f}_i, \mathbf{f}_j)$ . As the PPP-loss in Eq. 3 requires a similarity measure instead of a distance measure, we employ the complementary normalized cosine similarity  $\cos \angle(\mathbf{f}_i, \mathbf{f}_j) = \mathbf{f}_i^T \mathbf{f}_j$  with  $\|\mathbf{f}_i\| = \|\mathbf{f}_j\| = 1$ . Besides the desirable cluster-mean property of its complement, this metric is also efficient to calculate the distance matrix for the full batch using matrix multiplication libraries.

## 3 Experiments

### 3.1 Setup

**Datasets** This work comprises three balanced data streams: Split-MNIST, Split-CIFAR10 and Split-CIFAR100, and scrutinizes 10 highly unbalanced variants of the former two. Additionally, we examine two similar low-capacity setups in the Appendix. Each data stream is constituted by a sequence of tasks, each delineated by a subset of classes from the original dataset. Although the continual learner is completely ignorant to the notion of task, this setup enables careful evaluation of data streams with abrupt changes, which is most challenging in avoiding catastrophic forgetting compared to smooth and more iid task transitions. To ensure online processing of the data, only 1 epoch per task is allowed and a batch size  $|B_n|$  of 10 is adopted as in [25, 3, 23]. We use vanilla stochastic gradient descent, and all results are averaged over 5 different network initializations.

**Balanced data streams** contain a similar amount of data per task. We consider three benchmarks.

- **Split-MNIST** constitutes the MNIST [22] handwritten digit recognition dataset, split into 5 tasks according to pairs of incrementing digits. Each task comprises all original training data with 60k samples divided over the 5 tasks, and evaluation considers the full test subset.
- **Split-CIFAR10** considers the CIFAR10 [21] dataset, subdivided into 5 tasks with 2 labels each. Each task entails the full 10k training samples, with the entire test subset for evaluation.
- **Split-CIFAR100** is another variant of the CIFAR dataset with 100 different classes. The 50k training samples are subdivided in 20 tasks of 2.5k samples as in [25, 23].

**Unbalanced data streams.** Literature mostly assumes balanced data streams, whereas we scrutinize a more realistic scenario without equality assumptions on the task length. The data stream  $S$  comprises factor 10 more data in task  $T_i$ , denoted by  $S(T_i)$ . We consider all variants  $S(T_i)$ ,  $\forall i \in \{1, \dots, 5\}$  for both Split-MNIST and Split-CIFAR10. Following [3], Split-MNIST has 2k samples in  $T_i$ , whereas tasks  $T_j$  for  $j \neq i$  contain 0.2k samples. Further, we define unbalanced Split-CIFAR10 with 4k samples in  $T_i$ , and 0.4k samples in remaining tasks.

**Shared head.** These task-free setups contain no task information at both training and prediction. In contrast, previous task-incremental setups [7] typically use the task information to select the task-specific predictor head, while other heads remain fixed. This strong assumption trivializes prediction to a reduced discrete prediction space and neglects inter-head inference during training.

**Architectures.** MNIST setups use an MLP with 2 hidden layers of 400 units with 2k memories for the balanced setup as in [16, 23, 34], and 100 units with  $|\mathcal{M}| = 0.3k$  for the unbalanced setup as in [3]. Following [25], CIFAR setups use a slim version of Resnet18 [14] with a 1k memory size for CIFAR10 [3, 23], and 5k for CIFAR100 similar to [25].<sup>1</sup>

### 3.2 Methods

We consider a total of 10 baselines to compare our work with, explained in more detail below. The iid methods are not considered continual learning and GEM and iCaRL require task information.

**Reference baselines** define worst and most optimistic performance targets with a softmax classifier. The upper reference point for performance when relaxing the challenging non-iid feature in continual learning is set by **iid-online & iid-offline**. The full data stream  $S$  is shuffled to ensure the iid property, for which *iid-online* trains a single epoch and *iid-offline* multiple epochs, hence disregarding the online processing property. In contrast, the **finetune** baseline does learn from the non-iid datastream  $S$ , but optimizes solely for the new batch which typically results in worst-case catastrophic forgetting.

**Task incremental** baselines use task information during training. **GEM** [25] uses replay in a constraint optimization perspective to project gradients towards a local joint task optimum. Memory is equally divided over all tasks a priori, requiring task boundaries to allocate the memories. **iCaRL** [32] employs exemplars for knowledge distillation, with new task exemplars stored in a queue to optimally represent the class mean in feature space. Nearest mean prediction is possible only after fully learning the task by determining the exemplar based class means. Task boundaries set the recalculation point for knowledge distillation outputs and storing the exemplars in the dynamically subdivided memory.

**Task-free experience replay** baselines replay exemplars from an episodic memory. **Reservoir** [35] is a strong Experience Replay (ER) baseline with strong potential to outperform continual learning methods [6]. Samples are stored in memory  $\mathcal{M}$  with probability  $M/n$ , with  $n$  the number of observed samples and buffer size  $M$ . The buffer population tends to approximately follow the data stream distribution, severely deteriorating performance of underrepresented tasks in unbalanced data streams, as shown in Section 4.2. **MIR** [2] also uses an ER buffer, but extends retrieval to a loss-based strategy. This requires additional forward passes to attain the losses from a subset of samples. **GSS** [3] extends the GEM constraint optimization perspective to an instance-based level, adding samples to the buffer based on their gradients.

**Task-free model expansion** baselines extend the continual learner’s capacity. **CURL** [31] enables task-free and unsupervised adaptation using a multi-component Variational Auto-Encoder (VAE). Generative replay from a model-copy avoids forgetting in the current model. **CN-DPM** [23] is an expansion-based task-free method where subsets of the data are allocated to an expert network following a Dirichlet process mixture.

<sup>1</sup> Appendix details the full setup with additional experiments. Code publicly released upon paper acceptance.

## 4 Results and discussion

### 4.1 Balanced data streams

The results for the three balanced data streams in Table 1 consistently report state-of-the-art for our prototypical approach. In Split-MNIST, we close the gap to iid-online performance by 0.7% compared to main competitors GEM and DN-CPM, with our representations visualized in Figure 2. Furthermore, in the more challenging Split-CIFAR10 setup we significantly increase the gained margin by 3.7%. Finally, in Split-CIFAR100 we surpass the MIR and DN-CPM methods, and saliently outperform the iid-online baseline by 1.52%.

The difficulty for learning online is reflected in the discrepancy of performance between iid-offline and iid-online, which is a minimal 2% for Split-MNIST, strikingly increasing by factor 10 for Split-CIFAR10, and culminating to 30% in Split-CIFAR100.

Considering the baselines, GEM deteriorates for the Split-CIFAR10 data stream, similar to findings in [2, 3]. As a consequence, iCaRL can significantly outperform GEM in Split-CIFAR10, but exhibits inferior performance for the two other data streams, as iCaRL is not designed for online learning. From the expansion-based methods DN-CPM is our closest competitor, whereas CURL is more suited for unsupervised learning and lacks behind. Reservoir performs on par with iid-online for Split-CIFAR100, with loss-based extension MIR consistently gaining small margin for significant additional computational cost. However, the unbalanced experiments in Section 4.2 show that full reservoir-based population of the buffer strongly relies on this assumption of equally sized tasks, which is unlikely to occur in real-world data streams.

Table 1: The three balanced data stream accuracies (%) with standard deviation over 5 initializations. Expansion-based methods CURL [31] and DN-CPM [23] report results from their original work.

	<b>Split-MNIST</b>	<b>Split-CIFAR10</b>	<b>Split-CIFAR100</b>
iid-offline	98.44 $\pm$ 0.02	83.02 $\pm$ 0.60	50.28 $\pm$ 0.66
iid-online	96.57 $\pm$ 0.14	62.31 $\pm$ 1.67	20.10 $\pm$ 0.90
finetune	19.75 $\pm$ 0.05	18.55 $\pm$ 0.34	3.53 $\pm$ 0.04
GEM	93.25 $\pm$ 0.36	24.13 $\pm$ 2.46	11.12 $\pm$ 2.48
iCaRL	83.95 $\pm$ 0.21	37.32 $\pm$ 2.66	10.80 $\pm$ 0.37
reservoir	92.16 $\pm$ 0.75	42.48 $\pm$ 3.04	19.57 $\pm$ 1.79
MIR	93.20 $\pm$ 0.36	42.80 $\pm$ 2.22	20.00 $\pm$ 0.57
GSS	92.47 $\pm$ 0.92	38.45 $\pm$ 1.41	13.10 $\pm$ 0.94
CURL [31]	92.59 $\pm$ 0.66	—	—
DN-CPM [23]	93.23 $\pm$ 0.09	45.21 $\pm$ 0.18	20.10 $\pm$ 0.12
CoPE (ours)	<b>93.94 <math>\pm</math> 0.20</b>	<b>48.92 <math>\pm</math> 1.32</b>	<b>21.62 <math>\pm</math> 0.69</b>

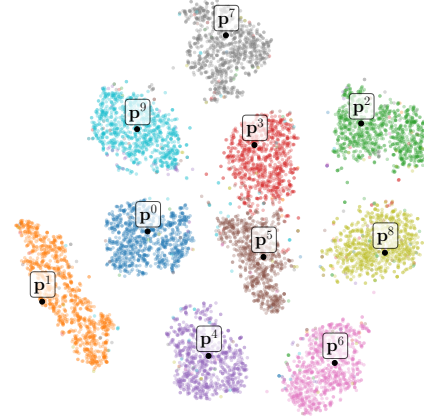


Figure 2: Balanced Split-MNIST test data first seed t-SNE [26] representation.

### 4.2 Unbalanced data streams

We scrutinize highly unbalanced data streams, with one task  $T_i$  containing factor 10 more data than the remaining four tasks as in [3], hence  $T_i$  constitutes over 70% of the data stream  $S(T_i)$ . Figure 3 summarizes the results for unbalanced Split-MNIST and Split-CIFAR10 data streams, for which our method respectively attains 5.4% and 6.4% over the compared baselines. Aljundi et al. [3] address robustness of GSS to an unbalanced Split-MNIST data stream compared to reservoir sampling. However, the more challenging Split-CIFAR10 setup shows reservoir sampling to better withstand the unbalanced data stream over both GSS and MIR. In contrast, our method enhances robustness in both unbalanced setups by high margin, attaining significant and consistent gains in performance with small standard deviation over the five  $S(T_i)$  data stream variations.

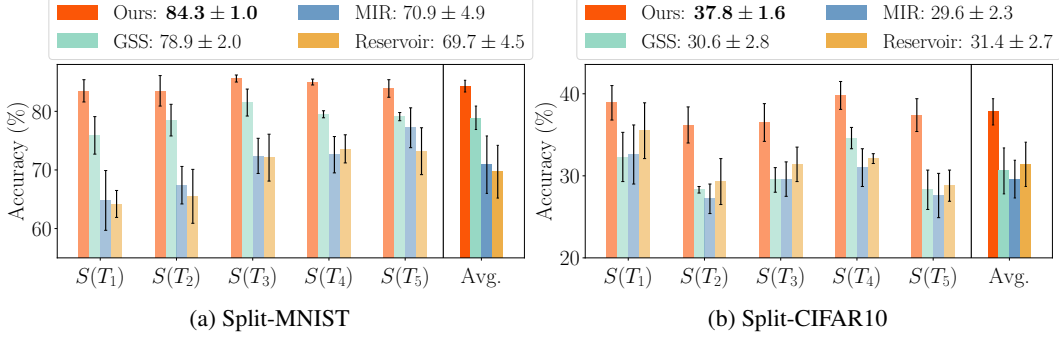


Figure 3: Unbalanced Split-MNIST (a) and Split-CIFAR10 (b) sequences  $S(T_i)$  with factor 10 more data in task  $T_i$ . Split-MNIST results for GSS reported from best of IQP/Greedy variants in [3].

### 4.3 PPP-loss analysis

In the challenging setting for online processing of non-iid data streams, the PPP-loss exploits information in the small batch  $B$ , introducing pseudo-prototypes  $\hat{\mathbf{p}}$  on top of the prototypes  $\mathbf{p}$ . This leads to questioning to what extent the pseudo-prototypes actually contribute to the quality of the embedding, and how this relates to the batch size.

We examine both inquiries in Table 2 for the three balanced data streams by comparing inclusion and exclusion of the pseudo-prototypes  $\hat{\mathbf{p}}$  in the PPP-loss, and extending the batch size  $|B_n|$ . First, including the pseudo-prototypes significantly improves the nearest mean classifier performance for all three benchmarks, and especially for the harder CIFAR setups. Although both setups use batch information to update the prototypes following Eq. 1, it seems crucial to use additional pseudo-prototypes in the PPP-loss to improve latent class density.

Second, to justify the use of pseudo-prototypes in online continual learning, we scrutinize different batch sizes in Table 2. Smaller batch sizes of 10 and 20 show very similar results, with results deteriorating towards increasing batch sizes. The PPP-loss implements the expectation over the prototype and the pseudo-prototypes, assuming uniform distribution in Eq. 2 and Eq. 4. Although this assumption impedes significance of the prototype in Eq. 2 for increasingly higher batch sizes, it results in ideal robustness for small online processing batches. This ideally suits the online continual learning setup, and small batches maintain the additional benefit of more frequent prototype updates for the same amount of processed data.

Table 2: Accuracies for ablating pseudo-prototypes  $\hat{\mathbf{p}}$  in PPP-loss, and varying batch size.

	PPP-loss		Batch Size $ B_n $				
	incl. $\hat{\mathbf{p}}$	excl. $\hat{\mathbf{p}}$	10 (Online)	20	50	100	200
Split-MNIST	$93.9 \pm 0.2$	$92.4 \pm 0.6$	$93.9 \pm 0.2$	$93.9 \pm 0.6$	$93.7 \pm 0.3$	$93.1 \pm 0.6$	$89.3 \pm 0.5$
Split-CIFAR10	$48.9 \pm 1.3$	$41.3 \pm 2.0$	$48.9 \pm 1.3$	$48.4 \pm 1.9$	$43.4 \pm 2.7$	$37.4 \pm 3.0$	$37.0 \pm 1.3$
Split-CIFAR100	$21.6 \pm 0.7$	$16.3 \pm 0.7$	$21.6 \pm 0.7$	$21.7 \pm 0.7$	$16.5 \pm 0.4$	$13.8 \pm 0.5$	$11.2 \pm 0.4$

## 5 Prior work

### 5.1 Continual learning

Continually learning systems are able to learn with limited resources from data streams prone to severe distribution shifts. Early works in task incremental settings [20, 24, 1, 38, 27, 32, 25] divide the data streams in large discrete batches, called tasks. The significantly large batch of task data is simultaneously accessible for multiple epochs during training, which prevents swift adaptation to the new data, requires a lot of resources, and possibly impedes prediction for the new task while learning. Moreover, the task a sample belongs to is assumed to be known to the continual learner during training, and using a different predictor head per task, is even presumed disclosed at prediction. Domain and class-incremental learning instead assume a single head [16, 34], but nonetheless make

no assumptions on task awareness during training. For an extensive survey we refer to [7]. Increased interest in real-world applicability causes task-free online continual learning to receive upcoming attention. This setup invigorates challenging single head prediction without any task knowledge or assumptions on underlying task distributions, and processes small batches of the data stream in an online fashion. Learning from a stream of data resembles a more humanlike process, as stimuli are constantly perceived to acquire subsequent sets of skills.

The branch of replay-based methods store a subset of representative samples in memory, repeatedly resampled to rehearse previously acquired knowledge. iCaRL [32] first addressed the class-incremental setting, with GEM [25] focusing on online processing from a constrained optimization perspective. However, both methods are specifically designed for task based settings. Further work in task-free online continual learning addresses population [3] and selection [2] from the replay memories.

Another branch of works focuses on expansion of network capacity. CURL [31] is a multicomponent VAE, using generative replay to avoid catastrophic forgetting. Further, Lee et al. [23] use a Dirichlet process to train a set of experts for subsets of the data. The crux in this dynamic expansion of the continual learner is unbound allocation of resources and tweaking the static threshold that determines when to create additional network components. This is strongly determined by the difficulty of the data stream, whereas replay-based methods can straightforwardly attain better performance by increasing the memory size [25].

## 5.2 Representation learning

A body of work in continual learning, meta-learning and unsupervised learning find their roots in learning representations. In continual representation learning, iCaRL uses a softmax classifier during training, from which the learned representations serve the nearest mean classifier at prediction, using exemplars to recalculate class means after learning a task. Further, CURL aims to map latent representations back into the input space. In continual fact learning, Elhoseiny et al. [9] explore learning in a joint visual-semantic embedding. However, their method relies on a static semantic embedding, which is pretrained and remains fixed throughout the continual learner lifetime. In contrast to these works, our approach exploits continually evolving prototypical representations in the latent space to effectively temper catastrophic forgetting, with robustness to more real-world imbalanced data streams.

In few-shot meta-learning, Snell et al. [33] learn an embedding in which the prototype is best represented by the class mean of a few samples. Alternatively, unsupervised representation learning exploits instance-based approaches, mainly focusing on solving self-supervised predictive tasks to acquire good representations from the data structure. Wu et al. [36] store instance representations of the full dataset in a memory bank for later reuse. Storing all data for data streams is exactly what continual learners try to avoid, with typically no re-occurrence of the samples in the data stream. He et al. [13] employ a dictionary-like approach which disentangles the encoders for the queries and keys by means of a slowly progressing momentum encoder that stabilizes keys in latent space for the iid data. Whereas deep embedding learning most commonly considers pairs [11] and triplets [12] of samples, other work uses batch information in lifted structure embeddings [30]. Unsupervised work in the same vein exploits the current batch to learn instance-wise softmax embeddings [37]. Both approaches fully depend on the batch size, whereas our approach aggregates both decoupled prototypes and additional batch pseudo-prototypes to defy class interference in latent space. All aforementioned unsupervised and meta-learning approaches are specifically designed for iid data, hence highly prone to catastrophic forgetting of previously acquired knowledge in data streams. Our prototypical method addresses this challenging problem to learn representations continually from imbalanced and non-iid data streams.

## 6 Conclusion

In this work, we devised a task-free online continual learner, able to learn and predict in a continual fashion for non-stationary and imbalanced data streams. The architecture is inherently single-headed, allows an unlimited growth in the number of categories and disentangles catastrophic forgetting from the network to a decoupled set of prototypes. We empirically prove the efficacy of our prototypical approach and its robustness to these highly imbalanced streams of data. We hope to encourage research in this direction, focusing on applications beyond classification and learning without supervision.

## Broader Impact

Data capturing our high-entropic world becomes available at unprecedented rates, urging artificially intelligent systems to learn in a continual fashion. In high contrast with a major body of work, we explore the route towards learning from real-world non-stationary data streams that are typically highly imbalanced. Ten properties of the ideal continual learner are listed in [7] from which our system enables satisfying the eight properties concerning supervised data for classification. Therefore, a truly continual learner is within reach, as other works focus on the two remaining properties to extend continual learning outside classification [29], and adapt both to unsupervised data [31] and local user data for model personalization [8]. This closes the gap towards continually evolving systems in real-world applications, such as autonomous vehicles and robotics, and therefore greatly impacts ways for artificial intelligence to reside within our society.

Furthermore, systems that learn and process the world in a similar fashion as humans, are likely to ease human-machine interactions. Continual learning neural networks using experience replay of episodic memories have strong connections to biological cognition systems. For example in the brains of rodents, coordination between the hippocampus and neocortex allow replay of episodic memories during sleep [17], and quiet waking periods after learning [19]. Further, our prototypical approach resembles the use of representativeness heuristics in human cognition [18], where instances are matched to the most similar prototype that represents the salient features of the parent population.

Arguably, an artificial intelligent system that can keep learning from a virtually unlimited stream of data, opens doors to general artificial intelligence. However, as the learning agents are mostly constrained to perception tasks, further research is required to incorporate symbolic expert systems and machine cognition [5]. Nonetheless, the inexorable rapid progress and research in artificially intelligent systems is unequalled, urging its designers to contemplate responsibility towards guarantees in future societal safety.

## Acknowledgments and Disclosure of Funding

The authors would like to thank Thomas Verelst for insightful discussions and Laura Van Geert for proofreading.

## References

- [1] Aljundi, R., Babiloni, F., Elhoseiny, M., Rohrbach, M., and Tuytelaars, T. (2018). Memory aware synapses: Learning what (not) to forget. In *Proceedings of the European Conference on Computer Vision (ECCV)*, pages 139–154.
- [2] Aljundi, R., Belilovsky, E., Tuytelaars, T., Charlin, L., Caccia, M., Lin, M., and Page-Caccia, L. (2019a). Online continual learning with maximal interfered retrieval. In *Advances in Neural Information Processing Systems*, pages 11849–11860.
- [3] Aljundi, R., Lin, M., Goujaud, B., and Bengio, Y. (2019b). Gradient based sample selection for online continual learning. In *Advances in Neural Information Processing Systems*, pages 11816–11825.
- [4] Banerjee, A., Merugu, S., Dhillon, I. S., and Ghosh, J. (2005). Clustering with bregman divergences. *Journal of machine learning research*, 6(Oct):1705–1749.
- [5] Bengio, Y. (2017). The consciousness prior. *arXiv preprint arXiv:1709.08568*.
- [6] Chaudhry, A., Rohrbach, M., Elhoseiny, M., Ajanthan, T., Dokania, P. K., Torr, P. H., and Ranzato, M. (2019). Continual learning with tiny episodic memories. *arXiv preprint arXiv:1902.10486*.
- [7] De Lange, M., Aljundi, R., Masana, M., Parisot, S., Jia, X., Leonardis, A., Slabaugh, G., and Tuytelaars, T. (2019). A continual learning survey: Defying forgetting in classification tasks. *arXiv preprint arXiv:1909.08383*.
- [8] De Lange, M., Jia, X., Parisot, S., Leonardis, A., Slabaugh, G., and Tuytelaars, T. (2020). Unsupervised model personalization while preserving privacy and scalability: An open problem. *arXiv preprint arXiv:2003.13296*.

[9] Elhoseiny, M., Babiloni, F., Aljundi, R., Rohrbach, M., Paluri, M., and Tuytelaars, T. (2018). Exploring the challenges towards lifelong fact learning. In *Asian Conference on Computer Vision*, pages 66–84. Springer.

[10] Grossberg, S. (1982). *Studies of mind and brain : neural principles of learning, perception, development, cognition, and motor control*. Boston studies in the philosophy of science 70. Reidel, Dordrecht.

[11] Hadsell, R., Chopra, S., and LeCun, Y. (2006). Dimensionality reduction by learning an invariant mapping. In *2006 IEEE Computer Society Conference on Computer Vision and Pattern Recognition (CVPR'06)*, volume 2, pages 1735–1742. IEEE.

[12] Harwood, B., Kumar, B., Carneiro, G., Reid, I., Drummond, T., et al. (2017). Smart mining for deep metric learning. In *Proceedings of the IEEE International Conference on Computer Vision*, pages 2821–2829.

[13] He, K., Fan, H., Wu, Y., Xie, S., and Girshick, R. (2019). Momentum contrast for unsupervised visual representation learning. *arXiv preprint arXiv:1911.05722*.

[14] He, K., Zhang, X., Ren, S., and Sun, J. (2016). Deep residual learning for image recognition. In *Proceedings of the IEEE conference on computer vision and pattern recognition*, pages 770–778.

[15] Hinton, G., Vinyals, O., and Dean, J. (2015). Distilling the knowledge in a neural network. *arXiv preprint arXiv:1503.02531*.

[16] Hsu, Y.-C., Liu, Y.-C., Ramasamy, A., and Kira, Z. (2018). Re-evaluating continual learning scenarios: A categorization and case for strong baselines. *arXiv preprint arXiv:1810.12488*.

[17] Ji, D. and Wilson, M. A. (2007). Coordinated memory replay in the visual cortex and hippocampus during sleep. *Nature neuroscience*, 10(1):100–107.

[18] Kahneman, D. and Tversky, A. (1972). Subjective probability: A judgment of representativeness. *Cognitive psychology*, 3(3):430–454.

[19] Karlsson, M. P. and Frank, L. M. (2009). Awake replay of remote experiences in the hippocampus. *Nature neuroscience*, 12(7):913.

[20] Kirkpatrick, J., Pascanu, R., Rabinowitz, N., Veness, J., Desjardins, G., Rusu, A. A., Milan, K., Quan, J., Ramalho, T., Grabska-Barwinska, A., et al. (2017). Overcoming catastrophic forgetting in neural networks. *Proceedings of the national academy of sciences*, 114(13):3521–3526.

[21] Krizhevsky, A., Hinton, G., et al. (2009). Learning multiple layers of features from tiny images.

[22] LeCun, Y., Bottou, L., Bengio, Y., and Haffner, P. (1998). Gradient-based learning applied to document recognition. *Proceedings of the IEEE*, 86(11):2278–2324.

[23] Lee, S., Ha, J., Zhang, D., and Kim, G. (2020). A neural dirichlet process mixture model for task-free continual learning. *arXiv preprint arXiv:2001.00689*.

[24] Li, Z. and Hoiem, D. (2017). Learning without forgetting. *IEEE transactions on pattern analysis and machine intelligence*, 40(12):2935–2947.

[25] Lopez-Paz, D. and Ranzato, M. (2017). Gradient episodic memory for continual learning. In *Advances in Neural Information Processing Systems*, pages 6467–6476.

[26] Maaten, L. v. d. and Hinton, G. (2008). Visualizing data using t-sne. *Journal of machine learning research*, 9(Nov):2579–2605.

[27] Mallya, A. and Lazebnik, S. (2018). Packnet: Adding multiple tasks to a single network by iterative pruning. In *Proceedings of the IEEE Conference on Computer Vision and Pattern Recognition*, pages 7765–7773.

[28] Mensink, T., Verbeek, J., Perronnin, F., and Csurka, G. (2013). Distance-based image classification: Generalizing to new classes at near-zero cost. *IEEE transactions on pattern analysis and machine intelligence*, 35(11):2624–2637.

[29] Michieli, U. and Zanuttigh, P. (2019). Incremental learning techniques for semantic segmentation. In *Proceedings of the IEEE International Conference on Computer Vision Workshops*, pages 0–0.

[30] Oh Song, H., Xiang, Y., Jegelka, S., and Savarese, S. (2016). Deep metric learning via lifted structured feature embedding. In *Proceedings of the IEEE conference on computer vision and pattern recognition*, pages 4004–4012.

[31] Rao, D., Visin, F., Rusu, A., Pascanu, R., Teh, Y. W., and Hadsell, R. (2019). Continual unsupervised representation learning. In *Advances in Neural Information Processing Systems*, pages 7645–7655.

[32] Rebuffi, S.-A., Kolesnikov, A., Sperl, G., and Lampert, C. H. (2017). icarl: Incremental classifier and representation learning. In *Proceedings of the IEEE conference on Computer Vision and Pattern Recognition*, pages 2001–2010.

[33] Snell, J., Swersky, K., and Zemel, R. (2017). Prototypical networks for few-shot learning. In *Advances in neural information processing systems*, pages 4077–4087.

[34] van de Ven, G. M. and Tolias, A. S. (2019). Three scenarios for continual learning. *arXiv preprint arXiv:1904.07734*.

[35] Vitter, J. S. (1985). Random sampling with a reservoir. *ACM Transactions on Mathematical Software (TOMS)*, 11(1):37–57.

[36] Wu, Z., Xiong, Y., Yu, S. X., and Lin, D. (2018). Unsupervised feature learning via non-parametric instance discrimination. In *Proceedings of the IEEE Conference on Computer Vision and Pattern Recognition*, pages 3733–3742.

[37] Ye, M., Zhang, X., Yuen, P. C., and Chang, S.-F. (2019). Unsupervised embedding learning via invariant and spreading instance feature. In *Proceedings of the IEEE Conference on Computer Vision and Pattern Recognition*, pages 6210–6219.

[38] Zenke, F., Poole, B., and Ganguli, S. (2017). Continual learning through synaptic intelligence. In *Proceedings of the 34th International Conference on Machine Learning-Volume 70*, pages 3987–3995. JMLR. org.

## Appendix

### A Algorithm

Our proposed algorithm is fully formalized in this section, as well as in our code that will be made publicly available on acceptance of this paper. Algorithm 1 and Algorithm 2 describe the training process for our continual learner, whereas  $c^* = \arg \max_{c \in C} \mathbf{f}_i^T \mathbf{p}^c$  is used for prediction, classifying  $\mathbf{x}_i$  as category  $c^*$  with the most similar prototype  $\mathbf{p}^{c^*}$ . As for a true continual learner, prediction is possible at any point in time, while the system keeps learning from the data stream.

---

**Algorithm 1** Training in the prototypical task-free online continual learning setup.

---

**Require:** data-stream  $S$ , prototype momentum  $\alpha$ , memory capacity  $M$ , learning rate  $\eta$   
**Initialize** replay memory  $\mathcal{M} = \emptyset$ , prototype memory  $\mathcal{P} = \emptyset$ , observed classes  $C = \emptyset$ , sample count per class  $N = \emptyset$ , model parameters  $\theta$

- 1: **for**  $B_n = \{(\mathbf{x}_1, y_1), \dots, (\mathbf{x}_{|B|}, y_{|B|})\} \sim S$  **do** ▷ Data stream batch w/o task information
- 2:    $B_{\mathcal{M}} \leftarrow \text{RANDOMSAMPLE}(\mathcal{M}, |B_n|)$  ▷ Randomly sample  $|B_n|$  exemplars from  $\mathcal{M}$
- 3:    $\mathcal{B} = \emptyset$
- 4:   **for**  $(\mathbf{x}_i, y_i) \in B_n \cup B_{\mathcal{M}}$  **do**
- 5:     **if**  $y_i \notin C$  **then**
- 6:       INITCLASS( $\mathcal{M}, \mathcal{P}, N, C, y_i$ ) ▷ Initialize memory and prototype
- 7:     **end if**
- 8:      $\mathcal{B} \leftarrow \mathcal{B} \cup f_{\theta}(\mathbf{x}_i)$  ▷ Collect features
- 9:   **end for**
- 10:   PROTOTYPEUPDATE( $\mathcal{P}, \mathcal{B}, N, \alpha$ ) ▷ Update prototypes in  $\mathcal{P}$
- 11:   MEMORYUPDATE( $\mathcal{M}, B_n, N$ ) ▷ Update memory  $\mathcal{M}$  with new input samples
- 12:    $J \leftarrow 0$  ▷ Initialize loss
- 13:   **for**  $\mathbf{f}_i^c \in \mathcal{B}$  **do**
- 14:      $J \leftarrow J - \frac{1}{|\mathcal{B}|} \left[ \log P(c|\mathbf{x}_i^c) + \sum_{\mathbf{x}_j^k} \log(1 - P(c|\mathbf{x}_j^k)) \right]$  ▷ Sum al instances PPP-loss
- 15:   **end for**
- 16:    $\theta \leftarrow \theta + \eta \nabla J$  ▷ Optimize objective with SGD
- 17: **end for**

---

**Algorithm 2** Memory Management of the replay memory and prototypes. UNIFORM $^{\mathbb{R}^d}(s_1, s_2)$  samples elements in a  $d$ -dimensional vector with uniform probability in range  $[s_1, s_2] \in \mathbb{R}$ .

---

**Require:** memory capacity  $M$

- 1: **function** INITCLASS( $\mathcal{M}, \mathcal{P}, N, C, k$ )
- 2:    $N \leftarrow N \cup \{N^k = 0\}$  ▷ Sample counts
- 3:    $C \leftarrow C \cup \{k\}$  ▷ Observed classes
- 4:    $\mathcal{M} \leftarrow \mathcal{M} \cup \{\mathcal{M}^k = \emptyset\}$
- 5:    $m = M/|C|$  ▷ Capacity per class
- 6:   **for**  $\mathcal{M}^c = (\mathbf{x}_1, \dots, \mathbf{x}_{|\mathcal{M}^c|}) \in \mathcal{M}$  **do**
- 7:      $\mathcal{M}^c \leftarrow (\mathbf{x}_1, \dots, \mathbf{x}_m)$  ▷ Keep first  $m$
- 8:      $\mathbf{p}^c \leftarrow \text{UNIFORM}^d(0, 1)$
- 9:      $\mathcal{P} \leftarrow \mathcal{P} \cup \{\mathbf{p}^c / \|\mathbf{p}^c\|_2\}$
- 10:   **end for**
- 11: **end function**

**function** PROTOTYPEUPDATE( $\mathcal{P}, \mathcal{B}, N, \alpha$ )

- 2:   **for**  $\mathbf{p}^c \in \mathcal{P}$  **do**
- 3:      $N^c \leftarrow N^c + |\mathcal{B}^c|$
- 4:      $\bar{\mathbf{p}}^c = \frac{1}{|\mathcal{B}^c|} \sum_{\mathbf{f}^c \in \mathcal{B}^c} \mathbf{f}^c$
- 5:      $\mathbf{p}^c \leftarrow \alpha \mathbf{p}^c + (1 - \alpha) \bar{\mathbf{p}}^c$
- 6:   **end for**
- 7: **end function**

**function** MEMORYUPDATE( $\mathcal{M}, B_n, N$ )

- 8:   **for**  $\mathbf{x}_i^c \in B_n$  **do** ▷ Class Reservoir
- 9:      $j = \text{UNIFORM}^{\mathbb{N}^1}(1, N^c)$
- 10:     **if**  $j \leq |\mathcal{M}^c|$  **then**
- 11:        $\mathcal{M}^c \leftarrow \mathbf{x}_i^c$
- 12:     **end if**
- 13:   **end for**
- 14: **end function**
- 15: **end function**

---

## B Setup

A gridsearch in the online continual learning setup was adopted, selecting the setup with highest performance, similar to [5]. All methods are prone to learning rate gridsearch  $[0.05, 0.01, 0.005, 0.001]$ . iCaRL knowledge distillation strength is set to 1, and GEM bias is set to 0.5, following [5, 7, 2]. GSS and MIR follow their original setup from their codebase in [2] and [1], with our additional learning rate gridsearch. CURL [6] and DN-CPM [4] results are reported from their original works. Our method also searched for a suitable temperature  $\tau = [0.1, 0.2, \dots, 1, 2]$  which was set to 0.1 for all balanced and unbalanced Split-MNIST and Split-CIFAR10 experiments, similar to [8]. Based on the ablation we set the prototypical momentum fixed to 0.99. For the challenging Split-CIFAR100 setting methods are allowed multiple iterations per batch as in [5], from which the best results are selected. The CIFAR100 temperature required higher concentration with  $\tau = 0.05$  and prototypical momentum 0.9. The latent dimensionality  $d$  in our setup is fixed to 100 for Split-MNIST as in [6], and selected 256 in a gridsearch [128, 256] and [128, 256, 512] for Split-CIFAR10 and Split-CIFAR100 respectively. We will make our code publicly available upon acceptance of this paper to ensure reproducibility.

## C Resource analysis task-free replay methods

In this section we compare usage of computational and memory resources for the replay methods fitted for the task-free online continual learning paradigm.

**Reservoir** is a powerful baseline for balanced data streams [3], with only minimal computational cost by keeping count  $n$  of how many samples have been observed. This count is then used relative to the buffer size  $M$  to define the probability  $M/n$  to store the new sample. As shown in the unbalanced data stream experiments, Reservoir is not fit for more real-world scenarios in which the assumption of equal frequency of occurrence per class typically doesn't hold. Improving this simple experience replay has led to research focusing on more complex strategies, as in the following.

**MIR** [1] replaces the random retrieval from the buffer in Reservoir with a loss-based approach. They store a momentary update of the network optimized for the new incoming batch and calculate the change in loss for a random subset of the replay memory  $\tilde{B}$ , which is larger than the buffer size (ideally five times the batch size for their experiments [1]). Besides a copy of the full model, this also requires calculating the loss twice in a sequential manner for the full subset  $\tilde{B}$  and an extra model update using only the new batch  $B_n$ , both significantly increasing processing time during training.

**GSS** [2] resides with Reservoir to use random retrieval of the buffer, but proposes a gradient-based population strategy. They introduce two variants, in which the first solves an Integer Quadratic Problem (IQP) with polynomial complexity w.r.t. the replay memory. As this is not scalable, they also propose a stochastic GSS-greedy variant. This more efficient GSS-greedy approach requires an additional forward pass, loss calculation, and backwards pass to obtain the gradients for the full considered subset  $\tilde{B}$  in the memory. Further, it requires similarities to serve the purpose for stochastic sample selection for the buffer. This also strains the memory requirements as batch  $B_n$  requires  $|B_n|$  times  $|\tilde{B}| + 1$  gradients to be accessed simultaneously to calculate  $|\tilde{B}|$  cosine similarities of the high-dimensional gradient-space.

**Our prototypical approach** resembles Reservoir's memory population by keeping count of the samples per class-specific memory subset  $\mathcal{M}^c$ . The PPP-loss requires calculation of a distance matrix with all the  $d$ -dimensional representations in the batch  $B$ . Using a normalized cosine similarity, this implies efficient matrix multiplication with the low-dimensional vectors. This is in high contrast to GSS, which calculates cosine similarity in the full high-dimensional gradient space for additional samples that are not present in current batch  $B$ , and therefore requires additional costly forward and backward passes. Furthermore, in our prototypical approach the prototype momentum updates also rely solely on samples that are in the current batch  $B$ , hence requiring only minimal computation. Comparing to both MIR and GSS, we don't require storing model copies or additional gradients, but merely store low-dimensional prototypes for each class, which gives a significant advantage in required storage space. For example, a Resnet18 model requires 11.7 million parameters to enable model copies or gradients, whereas our method even for 1000-way classification with  $d = 1024$  would require only 9% of the model capacity in memory for the prototypes.

## D Extended ablation study

### D.1 Ablation prototype momentum

In all our setups we employ a high momentum to update prototypes with the latent mean of the batch. Table 1 illustrates the influence of higher momentum ( $\geq 0.9$ ). Compared to low momentum of 0.1, Split-MNIST only gains a small margin of 0.45%, whereas Split-CIFAR10 and Split-CIFAR100 significantly improve with at least 3.0% and 4.2% respectively. Using momentum prevents the prototype to rely solely on the current batch instances, and higher momentum values attain a gradual change of the prototypes by stabilizes its trajectory in the ever evolving latent space.

Table 1: Ablation of momentum update for the prototypes. Higher momentum values ( $\geq 0.9$ ) obtain better results, especially for the CIFAR sequences, compared to low momentum (0.1).

Prototype Momentum				
	0.1	0.9	0.95	0.99
Split-MNIST	$93.49 \pm 0.70$	$94.11 \pm 0.34$	$93.96 \pm 0.30$	$93.94 \pm 0.20$
Split-CIFAR10	$44.48 \pm 3.19$	$48.02 \pm 2.49$	$47.98 \pm 3.14$	$48.92 \pm 1.32$
Split-CIFAR100	$15.79 \pm 1.16$	$21.62 \pm 0.69$	$21.56 \pm 0.58$	$20.01 \pm 1.81$

### D.2 Ablation inter and intra-class variance terms PPP-loss

In this section we scrutinize the importance in the two loss components to enhance inter and intra-class variance. We compare using only positive pairs from the batch (*pos*) or only negative pairs (*neg*) to the full-fledged PPP-loss (*joint*) in Table 2. The *pos* term shows competitive performance to the *joint* for Split-MNIST, but deteriorates as the data streams become harder for the CIFAR setups. The *neg* term is on par with the full PPP-loss for Split-MNIST and Split-CIFAR10, but collapses for Split-CIFAR100. The latter is challenging due to the high number of classes with only a batch size of 10, which impedes having psuedo-prototypes of all classes in the same batch. The *joint* incorporates both reduction of intra-class with the *pos* term and increases inter-class variance with the *neg* term, attaining state-of-the-art performance.

Table 2: Both checking the influence of both terms in the loss

PPP-loss			
	<i>joint</i>	<i>pos.</i>	<i>neg.</i>
Split-MNIST	$93.94 \pm 0.20$	$93.25 \pm 0.22$	$93.84 \pm 0.48$
Split-CIFAR10	$48.92 \pm 1.32$	$30.96 \pm 3.58$	$49.30 \pm 3.57$
Split-CIFAR100	$21.62 \pm 0.69$	$15.85 \pm 0.34$	$9.43 \pm 0.94$

### D.3 Pseudo-prototype ablation visualization

In the main paper we find in an ablation study that using pseudo-prototypes  $\hat{p}$  as proxy for the class-mean has significant improvements for the PPP-loss. Additionally, Figure 1 shows this in a 2-dimensional t-SNE space for the first seed of the balanced Split-MNIST experiment. Including the pseudo-prototypes (*incl.*  $\hat{p}$ ) illustrates a striking degree of inter-class variance in Figure 1a, whereas more interference occurs when excluding the pseudo-prototypes in Figure 1b. This is reflected in the performance, as including prototypes results in 94.52% accuracy, whereas excluding them has only 90.86% for the first seed.

## E Additional experiments

### E.1 Balanced data streams with low capacity

In these experiments we scrutinize performance of our prototypical approach compared to state-of-the-art methods, with less capacity in the memory and model and shorter data streams. All methods

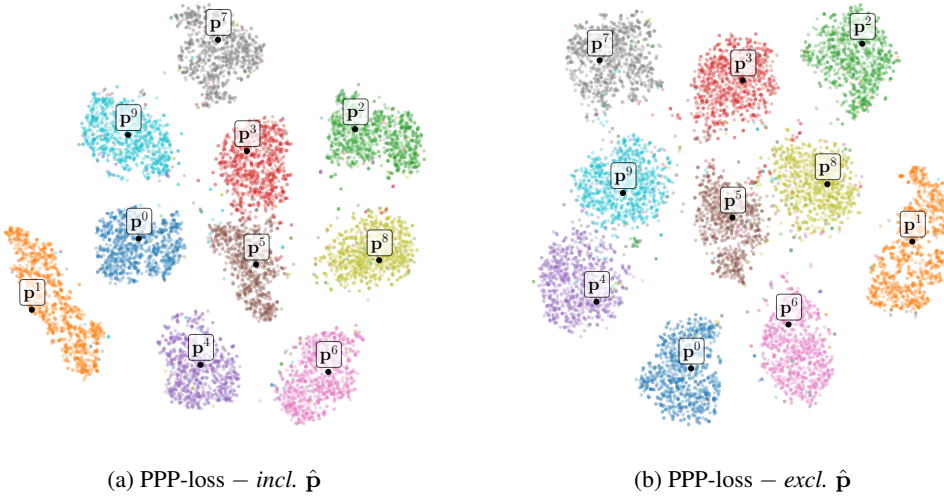


Figure 1: Split-MNIST first seed t-SNE representation of the test data, including (a) and excluding (b) the pseudo-prototypes  $\hat{\mathbf{p}}$  in the PPP-loss.

are allowed multiple iterations (maximal 5) as in [2]. Results are averaged over 5 seeds. Similar to the setup of GSS [2], we adopt two data sequences with truncated data per task:

- **Split-MNIST-mini** is similar to the Split-MNIST data stream with 5 tasks, but each task is confined to 1k training samples. Evaluation considers the full test subset. The network is an MLP with two hidden layers of 100 units, with total memory size of 0.3k exemplars. Latent dimensionality  $d$  is selected 32 from [16, 32, 64].
- **Split-CIFAR10-mini** is similar to the Split-CIFAR10 data stream with 5 tasks, but each task comprises 2k training samples, with a total subset of 10k samples out of the 50k available. The full test subset is used for evaluation. The network used is the same ResNet18 as in the main paper, with total memory size of 1k exemplars. Latent dimensionality  $d$  is selected 128 from [128, 256].

**Analysis** Table 3 shows the results for Split-MNIST-mini and Split-CIFAR10-mini, with GSS and DN-CPM results reported from their original works in a corresponding setup. In Split-MNIST-mini our method approaches the iid-online baseline with only 1.03% off, and 1.45% better than its closest competitors GEM and MIR.

In Split-CIFAR10-mini our approach saliently surpasses the iid-online baseline with 2.25%. Reservoir proves a strong baseline, with in this case the additional MIR loss-based retrieval decreasing performance. Similar to our findings in the main paper and [1, 2], GEM encounters difficulties in a CIFAR10 based setup, for which we find the bias hyperparameter  $\gamma \geq 0$  in the gradient projection to have insignificant influence.

## E.2 Unbalanced Benchmark Results

The graphs in the main paper visualize the numbers in Table 4, which we fully report here as a reference for future work. Each  $S(T_i)$  data stream performance is averaged over five different initial seeds. The ‘Avg.’ results average over all mean performances of the dataset variants  $S(T_i), \forall i \in \{1, \dots, 5\}$ .

## References

- [1] Aljundi, R., Belilovsky, E., Tuytelaars, T., Charlin, L., Caccia, M., Lin, M., and Page-Caccia, L. (2019a). Online continual learning with maximal interfered retrieval. In *Advances in Neural Information Processing Systems*, pages 11849–11860.
- [2] Aljundi, R., Lin, M., Goujaud, B., and Bengio, Y. (2019b). Gradient based sample selection for online continual learning. In *Advances in Neural Information Processing Systems*, pages 11816–11825.

Table 3: Split-MNIST-mini and Split-CIFAR10-mini results, with only 1k and 2k samples per task. GSS [2] and DN-CPM [4] results reported from original work in these setups.

	<b>Split-MNIST-mini</b>	<b>Split-CIFAR10-mini</b>
iid-offline	$94.58 \pm 0.17$	$67.41 \pm 1.37$
iid-online	$87.57 \pm 3.54$	$42.50 \pm 2.15$
finetune	$21.74 \pm 3.38$	$16.65 \pm 0.24$
GEM	$85.09 \pm 0.52$	$22.31 \pm 1.37$
iCaRL	$83.23 \pm 0.92$	$26.54 \pm 2.73$
reservoir	$82.73 \pm 2.39$	$38.21 \pm 3.39$
MIR	$84.40 \pm 0.91$	$37.20 \pm 2.74$
GSS [2]	$82.60 \pm 2.90$	$33.56 \pm 1.70$
DN-CPM [4]	—	$41.78$
Ours	<b><math>86.54 \pm 1.41</math></b>	<b><math>44.75 \pm 2.68</math></b>

Table 4: Unbalanced Split-MNIST and Split-CIFAR10 sequences  $S(T_i)$  with factor 10 more data in task  $T_i$ . Split-MNIST results for GSS reported from best of IQP/Greedy variants in [2].

Dataset	Unbalanced Sequence	Ours	GSS	MIR	Reservoir
<b>Split-MNIST</b>	$S(T_1)$	$83.5 \pm 1.9$	$75.9 \pm 3.2$	$64.8 \pm 5.1$	$64.2 \pm 2.3$
	$S(T_2)$	$83.5 \pm 2.6$	$78.5 \pm 2.7$	$67.4 \pm 3.2$	$65.5 \pm 4.6$
	$S(T_3)$	$85.6 \pm 0.6$	$81.5 \pm 2.3$	$72.4 \pm 3.0$	$72.1 \pm 4.0$
	$S(T_4)$	$85.0 \pm 0.5$	$79.5 \pm 0.6$	$72.6 \pm 3.1$	$73.6 \pm 2.4$
	$S(T_5)$	$83.9 \pm 1.5$	$79.1 \pm 0.7$	$77.2 \pm 3.4$	$73.2 \pm 4.0$
	Avg.	<b><math>84.3 \pm 1.0</math></b>	$78.9 \pm 2.0$	$70.9 \pm 4.9$	$69.7 \pm 4.5$
<b>Split-CIFAR10</b>	$S(T_1)$	$38.9 \pm 2.1$	$32.3 \pm 3.0$	$32.6 \pm 3.6$	$35.5 \pm 3.4$
	$S(T_2)$	$36.2 \pm 2.2$	$28.3 \pm 0.4$	$27.2 \pm 1.8$	$29.3 \pm 2.8$
	$S(T_3)$	$36.5 \pm 2.3$	$29.5 \pm 1.5$	$29.6 \pm 2.1$	$31.4 \pm 2.1$
	$S(T_4)$	$39.8 \pm 1.7$	$34.6 \pm 1.3$	$31.0 \pm 2.3$	$32.1 \pm 0.6$
	$S(T_5)$	$37.4 \pm 2.0$	$28.3 \pm 2.4$	$27.6 \pm 2.7$	$28.8 \pm 1.9$
	Avg.	<b><math>37.8 \pm 1.6</math></b>	$30.6 \pm 2.8$	$29.6 \pm 2.3$	$31.4 \pm 2.7$

- [3] Chaudhry, A., Rohrbach, M., Elhoseiny, M., Ajanthan, T., Dokania, P. K., Torr, P. H., and Ranzato, M. (2019). Continual learning with tiny episodic memories. *arXiv preprint arXiv:1902.10486*.
- [4] Lee, S., Ha, J., Zhang, D., and Kim, G. (2020). A neural dirichlet process mixture model for task-free continual learning. *arXiv preprint arXiv:2001.00689*.
- [5] Lopez-Paz, D. and Ranzato, M. (2017). Gradient episodic memory for continual learning. In *Advances in Neural Information Processing Systems*, pages 6467–6476.
- [6] Rao, D., Visin, F., Rusu, A., Pascanu, R., Teh, Y. W., and Hadsell, R. (2019). Continual unsupervised representation learning. In *Advances in Neural Information Processing Systems*, pages 7645–7655.
- [7] Rebuffi, S.-A., Kolesnikov, A., Sperl, G., and Lampert, C. H. (2017). icarl: Incremental classifier and representation learning. In *Proceedings of the IEEE conference on Computer Vision and Pattern Recognition*, pages 2001–2010.
- [8] Ye, M., Zhang, X., Yuen, P. C., and Chang, S.-F. (2019). Unsupervised embedding learning via invariant and spreading instance feature. In *Proceedings of the IEEE Conference on Computer Vision and Pattern Recognition*, pages 6210–6219.